JOURNAL OF THE AMERICAN CHEMICAL SOCIETY

Subscriber access provided by ISTANBUL TEKNIK UNIV

Article

Molecular Structure of Self-Assembled Chiral Nanoribbons and Nanotubules Revealed in the Hydrated State

Reiko Oda, Franck Artzner, Michel Laguerre, and Ivan Huc

J. Am. Chem. Soc., **2008**, 130 (44), 14705-14712 • DOI: 10.1021/ja8048964 • Publication Date (Web): 11 October 2008

Downloaded from http://pubs.acs.org on February 8, 2009

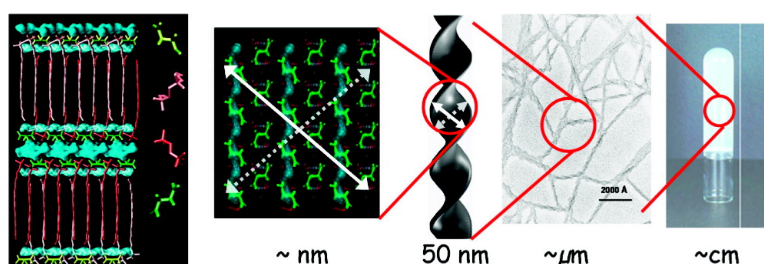

More About This Article

Additional resources and features associated with this article are available within the HTML version:

- Supporting Information
- Access to high resolution figures
- Links to articles and content related to this article
- Copyright permission to reproduce figures and/or text from this article

View the Full Text HTML

ACS Publications
High quality. High impact.

Journal of the American Chemical Society is published by the American Chemical Society. 1155 Sixteenth Street N.W., Washington, DC 20036

J|A|C|S
ARTICLES
Published on Web 10/11/2008

Molecular Structure of Self-Assembled Chiral Nanoribbons and Nanotubules Revealed in the Hydrated State

Reiko Oda,*,† Franck Artzner,*,‡ Michel Laguerre,† and Ivan Huc†

Institut Européen de Chimie et Biologie (IECB), Université de Bordeaux-CNRS, UMR 5248, 2 rue Robert Escarpit, F-33607 Pessac Cedex, France, and Institut de Physique de Rennes, Université Rennes 1, UMR-CNRS 6251, Campus Beaulieu Bat. 11A, 35042 Rennes Cedex, France

Received June 26, 2008; E-mail: r.oda@iecb.u-bordeaux.fr; franck.artzner@univ-rennes1.fr

Abstract: A detailed molecular organization of racemic 16-2-16 tartrate self-assembled multi-bilayer ribbons in the hydrated state is proposed where 16-2-16 amphiphiles, tartrate ions, and water molecules are all accurately positioned by comparing experimental X-ray powder diffraction and diffraction patterns derived from modeling studies. X-ray diffuse scattering studies show that molecular organization is not fundamentally altered when comparing the flat ribbons of the racemate to chirally twisted or helical ribbons of the pure tartrate enantiomer. Essential features of the three-dimensional molecular organizations of these structures include interdigitation of alkyl chains within each bilayer and well-defined networks of ionic and hydrogen bonds between cations, anions, and water molecules between bilayers. The detailed study of diffraction patterns also indicated that the gemini headgroups are oriented parallel to the long edge of the ribbons. The structure thus possesses a high cohesion and good crystallinity, and for the first time, we could relate the packing of the chiral molecules to the expression of the chirality at a mesoscopic scale. The organization of the ribbons at the molecular level sheds light on a number of their macroscopic features. Among these are the reason why enantiomerically pure 16-2-16 tartrate forms ribbons that consist of exactly two bilayers, and a plausible mechanism by which a chirally twisted or helical shape may emerge from the packing of chiral tartrate ions. Importantly, the distinction between commonly observed helical and twisted morphologies could be related to a subtle symmetry breaking. These results demonstrate that accurately solving the molecular structure of self-assembled soft materials—a process rarely achieved—is within reach, that it is a valid approach to correlate molecular parameters to macrocopic properties, and thus that it offers opportunities to modulate properties through molecular design.

Introduction

Chiral amphiphilic molecules often assemble in solution to form aggregates with high aspect ratios, such as rods, tapes, or tubes.[1,2] Their morphology frequently expresses the chirality of their components at a supramolecular scale of nanometers to micrometers; the fibrous structures may be coiled, twisted, or wound around one another, and exist as a left-handed or a right-handed form. On fundamental grounds, the relationship between molecular chirality (∼Å) and supramolecular chirality (∼μm) as expressed in these structures represents an excellent model for studying the emergence of specific shapes at a macroscopic scale through cooperative interactions between a large number of very small building blocks. In addition to this fundamental aspect, chiral fibrous objects possess a great potential for development of new functional supramolecular devices, taking advantage of the chirality of the molecular constituents organized in a hierarchical manner and/or of the supramolecular chirality of the fibers that can be generated. Examples of applications are for chiral recognition, using chiral fibers as templates for helical crystallization of proteins, or for the growth of inorganic replicas.[1–3]

One great challenge in this area is to understand the role of parameters such as cooperative hydrogen bonding and/or $\pi-\pi$ stacking which determine intermolecular interactions and thus the morphology of these remarkable chiral structures. Very often, the balance between these parameters is subtle because these assemblies result from the cooperative effects of multiple weak interactions between a large numbers of subcomponents; seemingly slight changes in the experimental conditions or molecular structures may lead to important changes of chiral fiber morphology. Among these, the most studied are twisted and helical ribbons of single or multiple bilayer membranes. Helical ribbons have a cylindrical curvature and can be precursors of tubules.[3–10] Twisted ribbons have Gaussian or

† Université de Bordeaux.
‡ Université Rennes 1.

(1) Ihara, H.; Takafuji, M.; Sakurai, T. In *Encyclopedia of Nanoscience and Nanotechnology*; Nalwa, H. S., Ed.; American Scientific Publishers: Stevenson Ranch, CA, 2004; Vol. 9, pp 473−495.
(2) Brizard, A.; Oda, R.; Huc, I. *Top. Curr. Chem.* **2005**, *256*, 167–218.
(3) Schnur, J. M. *Science* **1993**, *262*, 1669–1676.
(4) Yager, P.; Schoen, P. E. *Mol. Cryst. Liq. Cryst.* **1984**, *106*, 371–381.
(5) Georger, J. H.; Singh, A.; Price, R. R.; Schnur, J. M.; Yager, P.; Schoen, P. E. *J. Am. Chem. Soc.* **1987**, *109*, 6169–6175.
(6) Fuhrhop, J.-H.; Schnieder, P.; Boekema, E.; Helfrich, W. *J. Am. Chem. Soc.* **1988**, *110*, 2861–2867.
(7) Yanagawa, H.; Ogawa, Y.; Furuta, H.; Tsuno, K. *J. Am. Chem. Soc.* **1989**, *111*, 4567–4570.
(8) Kunitake, T.; Yamada, N. *Chem Commun* **1986**, 655–656.
(9) John, G.; Yoshida, K.; Shimizu, T. *J. Am. Chem. Soc.* **2002**, *124*, 10674–10675.

10.1021/ja8048964 CCC: $40.75 © 2008 American Chemical Society

saddle-like curvature.[11−14] These intriguing shapes can be simply visualized using microscopy and have fascinated both chemists and physicists. The expressed chirality ranges from tens of nanometers to micrometers, whereas molecular chirality is of the order of angstroms.[15] Therefore, the tilt or twist of a molecule with respect to neighboring molecules is generally very small, i.e., less than a degree.

Various theoretical approaches have been proposed to characterize the curvatures and morphologies of such membranes by calculating their elastic free energy in attempts to explain the correlation between the morphologies of the chiral ribbons and molecular organization.[4,16−21] Most of these models are inspired by continuous elastic models developed for mechanical deformation of liquid crystals. Particular effort has been made by several groups to investigating the difference between helical and twisted ribbons.[14,22,23] In all cases, these are based on the models treating the membranes as continuous media with given properties, and while they may allow us to qualitatively describe the structures, the lack of atomic details prohibits molecular design of new systems.

Many attempts have been made to elucidate molecular packing of self-assembled hydrated fibers at atomic resolution. Circular dichroism is a technique often used to shed light on chiral molecular organization. It allows for assessment of induced chirality and chirality amplification and sometimes permits the determination of the handedness of helical molecular packing in the fibers.[24] In principle, X-ray diffraction should provide more accurate information about molecular organization at close to atomic resolution if (and only if) the molecules have crystalline order. However, this remains a major hurdle because chiral self-assembled fibers are thin and “soft” materials without long three-dimensional crystalline order and are often labile in solution. Thus, except in a couple of cases,[25,26] studies on molecular organization within fibrous aggregates (chiral or not) have been performed on dried and desolvated fibers. Frequently, sharp diffraction peaks observed on dried fibers disappear upon their solvation and are not amenable to detailed determination of molecular packing. Therefore, the assumption is made that fibrous aggregates are in a pseudocrystalline state and that molecular organization is unchanged when the gels or the fibers are dried.[27−35] Meanwhile, the validity of such assumptions must be questioned in each case. Another assumption commonly made is that molecular packing within a soft gel fiber may be similar to the packing of the gelator or of its analogues in single crystals. Single-crystal structures determined by X-ray crystallography provide very accurate information about molecular packing.[35–38] However, while the analogy between fiber and single-crystal structures has sometimes been validated by comparison of the powder diffraction patterns, this control was not performed in many cases. Occasionally, it was even clearly demonstrated that a single-crystal structure and the corresponding gel structure do not match.[39]

Beyond the elucidation of the structure of self-assembled fibers at the molecular level, a second challenge lies in relating molecular packing to macroscopic features such as fiber shape and supramolecular chirality. In most cases, self-assembled fibers are very thin and have very low X-ray scattering intensity. The observation of an isolated fiber in order to determine the orientation of molecules with respect to the fiber coordinates remains very difficult, and measurements performed on ensembles of fibers give rise to powder diffraction that does not allow the orientation of molecular arrangements to be defined. Additionally, other techniques which allow the direct observation of isolated fibers (i.e., electron microscopy and atomic force microscopy, AFM) do not yet have the necessary resolution to observe molecular organization. Only in exceptional cases are the fibers large enough to be manipulated individually and possess single-crystal-like properties. For example, based on the knowledge on the 3D crystals of cholesterol monohydrate

(10) Shimizu, T.; Masuda, M.; Minamikawa, H. *Chem. Rev* **2005**, *105*, 1401–1443.
(11) Tachibana, T.; Kambara, H. *J. Am. Chem. Soc.* **1965**, *87*, 3015–3016.
(12) Nakashima, N.; Asakuma, S.; Kim, J.-M.; Kunitake, T. *Chem. Lett.* **1984**, 1709–1712.
(13) Oda, R.; Huc, I.; Candau, S. J. *Angew. Chem., Int. Ed.* **1998**, *37*, 2689–2691.
(14) Oda, R.; Huc, I.; Candau, S. J.; MacKintosh, F. C. *Nature* **1999**, *399*, 566–569.
(15) Jacques, J.; Collet, A.; Wilen, S. H. *Enantiomers, Racemates and Resolutions*, 3rd ed.; Krieger: Malabar, FL, 1994.
(16) Thomas, B. N.; Corcoran, R. C.; Cotant, C. L.; Lindemann, C. M.; Kirsch, J. E.; Persichini, P. J. *J. Am. Chem. Soc.* **1998**, *120*, 12178–12186.
(17) Helfrich, W. *Z. Naturforsch.* **1973**, *28C*, 693–703.
(18) de Gennes, P. G. *C. R. Acad. Sci. Paris* **1987**, *304*, 259–263.
(19) Komura, S.; Zhong-can, O.-Y. *Phys. Rev. Lett.* **1998**, *81*, 473–476.
(20) Lubensky, T. C.; Prost, J. *J. Phys. II* **1992**, *2*, 371–382.
(21) Aggeli, A.; Nyrkova, I. A.; Bell, M.; Harding, R.; Carrick, L.; Mcleish, T. C. B.; Semenov, A. N.; Boden, N *Proc. Natl. Acad. Sci. U.S.A.* **2001**, *98*, 11857–11862.
(22) (a) Selinger, J. V.; Schnur, J. M. *Phys. Rev. Lett.* **1993**, *71*, 4091–4094. (b) Selinger, J. V.; MacKintosh, E. C.; Schnur, J. M. *Phys. Rev. E* **1996**, *53*, 3804–3818. (c) Selinger, J. V.; Spector, M. S.; Schnur, J. M. *J. Phys. Chem. B* **2001**, *105*, 7158–7169.
(23) Tu, Z. C.; Seifert, U. *Phys. Rev. E* **2007**, *76*, 31603.
(24) (a) Gronwald, O.; Shinkai, S. *J. Chem. Soc., Perkin Trans. 2* **2001**, 1933–1937. (b) Kobayashi, H.; Friggeri, A.; Koumoto, K.; Amaike, M.; Shinkai, S.; Reinhoudt, D. N. *Org. Lett.* **2002**, 1423–1426. (c) de Jong, J. J. D.; Lucas, L. N.; Kellogg, L. M.; van Esch, J. H.; Feringa, B. L. *Science* **2004**, *304*, 278–281. (d) Iwaura, R.; Yoshida, K.; Masuda, M.; Ohnishi-Kameyama, M.; Yoshida, M.; Shimizu, T. *Angew. Chem., Int. Ed.* **2003**, *42*, 1009–1012.
(25) Abdallah, D. J.; Sirchio, S. A.; Weiss, R. G. *Langmuir* **2000**, *16*, 7558–7561.
(26) Yui, H.; Minamikawa, H.; Danev, R.; Nagayama, K.; Kamiya, S.; Shimizu, T. *Langmuir* **2008**, *24*, 709–713.
(27) Terech, P.; Rodriguez, V.; Barnes, J. D.; McKenna, G. B. *Langmuir* **1994**, *10*, 3406–3418.
(28) Estroff, L. A.; Leiserowitz, L.; Addadi, L.; Weiner, S.; Hamilton, A. D. *Adv. Mater.* **2003**, *15*, 38–42.
(29) Shimizu, T.; Masuda, M. *J. Am. Chem. Soc.* **1997**, *119*, 2812–2818.
(30) Gronwald, O.; Shinkai, S. *Chem. Eur. J.* **2001**, *7*, 4328–4334.
(31) Palui, G.; Simon, F. -X.; Schmutz, M.; Mesini, P. J.; Banerjee, A. *Tetrahedron* **2008**, *64*, 175–185.
(32) Yoshikawa, I.; Yanagi, S.; Yamaji, Y.; Araki, K. *Tetrahedron* **2007**, *63*, 7474–7481.
(33) Liu, Q.; Wang, Y.; Li, W.; Wu, L. *Langmuir* **2007**, *23*, 8217–8223.
(34) Lim, G. S.; Jung, B. M.; Lee, S. J.; Song, H. H.; Kim, C.; Chang, J. Y. *Chem. Mater.* **2007**, *19*, 460–467.
(35) Trivedi, D. R.; Dastidar, P. *Crystal Growth Design* **2006**, *6*, 2114–2121.
(36) Caffrey, M.; Hogan, J.; Rudolph, A. S. *Biochemistry* **1991**, *30*, 2134–2146.
(37) (a) Babu, P.; Sangeetha, N. M.; Vijaykumar, P.; Maitra, U.; Rissanen, K.; Raju, A. R. *Chem. Eur. J.* **2003**, *9*, 1922–1932. (b) Mamiya, J. I.; Kanie, K.; Hiyama, T.; Ikeda, T.; Kato, T. *Chem. Commun.* **2002**, 1870–1871. (c) Jokić, M.; Makarević, J.; Žinić, M. *J. Chem. Soc., Chem. Commun.* **1995**, 1723–1724. (d) Becceril, J.; Escuder, B.; Miravet, J. F.; Gavara, R.; Luis, S. V. *Eur. J. Org. Chem.* **2005**, 481–485. (e) Makarević, J.; Jokić, M.; Raza, Z.; Štefanić, Z.; Kojić-Prodić, B.; Žinić, M. *Chem. Eur. J.* **2003**, *9*, 5567–5580. (f) Menger, F. M.; Yamasaki, Y.; Catlin, K. K.; Nishimi, T. *Angew. Chem., Int. Ed. Engl.* **1995**, *34*, 585–586. (g) Snijder, C. S.; de Jong, J. C.; Meetsma, A.; van Bolhuis, F.; Feringa, B. L. *Chem. Eur. J.* **1995**, *1*, 549–597. (h) Shirakawa, M.; Kawano, S.; Fujita, N.; Sada, K.; Shinkai, S. *J. Org. Chem.* **2003**, *68*, 5037–5044.
(38) Ghosh, R.; Chakraborty, A.; Maiti, D. K.; Puranik, V. G. *Org. Lett.* **2006**, *8*, 1061–1064.
(39) Svenson, S.; Kirste, B.; Fuhrhop, J.-H. *J. Am. Chem. Soc.* **1994**, *116*, 11969–11975.

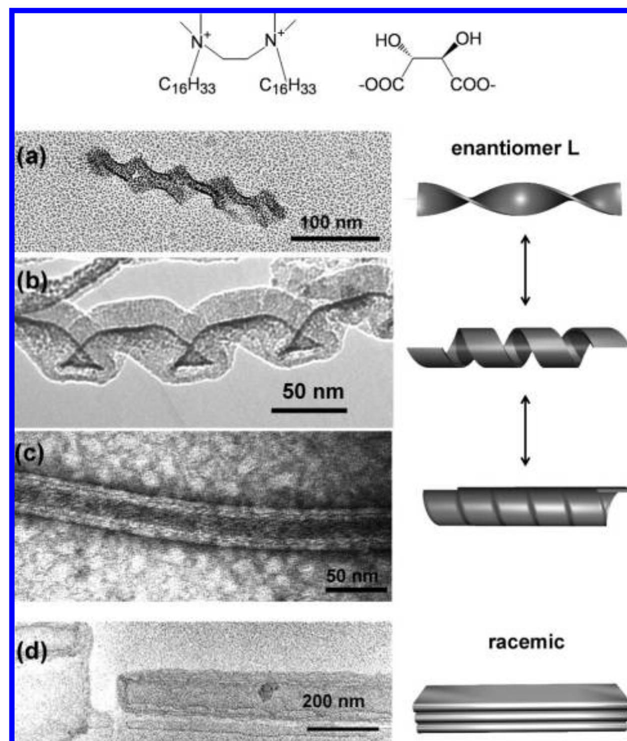

Figure 1. Formula of the 16-2-16 L-tartrate. Transmission electron microscopy (TEM) images and schematic representation of twisted ribbons (a), helical ribbons (b), and tubules (c) of 16-2-16 L-tartrate; TEM image and schematic representation of flat ribbons of racemic 16-2-16 tartrate (d). The morphologies of the multilayer ribbons depend on the ee of the tartrate counterion. For a pure enantiomer, twisted ribbons form first and transform into helical ribbons and tubules. This transformation into helical ribbons/tubules subsists at an ee as low as 0.8, but below ee = 0.6, only twisted ribbons are observed. The pitch of the twist increases with decreasing ee, up to an infinite value for ee = 0 (flat ribbon).

and on the diffraction pattern of individual micrometric fibers, Benedek et al. have resolved the molecular structure of cholesterol tubules.[40]

We have previously reported that nonchiral cationic gemini surfactants having the formula C_2H_4-1,2-($(CH_3)_2N^+C_{16}H_{33})_2$, denoted as 16-2-16, form twisted ribbons in solution in the presence of chiral tartrate counterions (Figure 1).[13,14] The handedness of the ribbons depends on the D or L chiral configuration of tartrate, and their twist pitch decreases continuously upon increasing the enantiomeric excess (ee). Chirality induction by the tartrates was shown to involve selective anion−cation recognition and conformationally labile chirality in the cations.[41] Recently, we also demonstrated that, depending on various parameters, not only do twisted ribbons form, but also helical ribbons evolve into tubules (Figure 1).[42]

Such a fine tunability of nanometric chiral assemblies is very intriguing, particularly considering that chirality in this system comes solely from counterions. It offers a versatile approach to prepare chiral nanoobjects. In order to shed light on the mechanism of chirality transfer from counterions to amphiphiles, and from molecular level to supramolecular level, we have

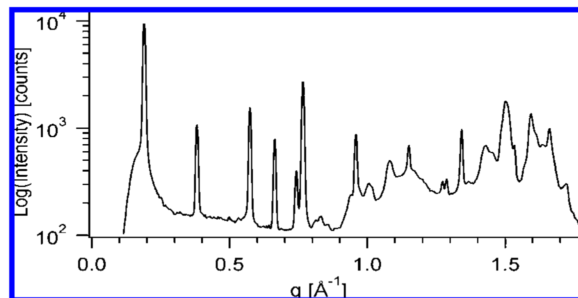

Figure 2. X-ray diffraction pattern of an aqueous suspension of flat ribbons of racemic 16-2-16 tartrate, 10% w/w at 20 °C.

carried out and now report an investigation of molecular packing at atomic resolution of the soft and hydrated, multilayered chiral assemblies of 16-2-16 tartrate molecules. We used a multiscale approach involving small-angle and wide-angle X-ray scattering (SAXS and WAXS) and molecular modeling to elucidate the molecular structures of three distinct morphologies of gemini tartrate ribbons: planar, twisted, and helical. The molecular packing was found to be very similar in all three structures, differing only by subtle symmetry breaking. It was clearly observed that the presence of solvent molecules (water) in the core of the crystalline structure is crucial for their cohesion but makes structure resolution extremely difficult. To the best of our knowledge, this is an unprecedented example in which three-dimensional molecular organization is elucidated in chiral membrane structures in the presence of solvent. The organization and the orientation of the chiral molecules could be determined with respect to the chiral ribbons with high aspect ratio, giving a clear indication of how the molecular chirality is translated at the mesoscopic level. These results give fundamental insights on the structure of such chiral assemblies. They also represent an important methodological progress, given the general difficulty in reaching atomic resolution in soft matter.

Results and Discussion

Crystallographic Analysis of the Multilayered Racemate Structure. Infrared spectroscopy of 16-2-16 DL-tartrate ribbons shows that the chains have orthorhombic crystalline ordering.[43] This also holds in twisted or helical ribbons as well as in tubules of the pure tartrate enantiomer.[42] As shown in the following, crystalline ordering was confirmed by high-resolution powder diffraction of these assemblies. The X-ray pattern of a white gel of racemic 16-2-16 tartrate in water (10% w/w) exhibits sharp peaks up to a resolution of 3.5 Å, i.e., $q = 1.8$ Å^{-1} (Figure 2 and Table 1), which could unambiguously be indexed in an orthorhombic 3D crystal lattice with $a = 65.16$ Å, $b = 7.77$ Å, $c = 9.84$ Å, and a unit cell volume $V = 4978$ Å^3. The first extinctions (Supporting Information, Table S1) of the peaks are in agreement with a non-centrosymmetric $Pna2_1$ space group (No. 33). The unit cell is constituted by four equivalent entities (asymmetric unit), each with a volume of 1244 Å^3, corresponding to a unique gemini/tartrate ion pair and some water. The four entities are linked by three symmetry elements associated with $Pna2_1$: two glide mirror planes, n and a, and a two-fold 2_1 screw axis.

The unit cell is long enough to span two bilayers linked by a glide mirror plane a oriented along (a,c) with an a/2 translation. The thickness of the bilayer of about a/2 (32.58 Å)

(40) Khaykovich, B.; Hossain, C.; McManus, J. J.; Lomakin, A.; Moncton, D. E.; Benedek, G. B. *Proc. Natl. Acad. Sci. U.S.A.* **2007**, *104*, 9656–9660.
(41) Berthier, D.; Buffeteau, T.; Leger, J.-M.; Oda, R.; Huc, I. *J. Am. Chem. Soc.* **2002**, *124*, 13486–13494.
(42) Brizard, A.; Aimé, C.; Labrot, T.; Huc, I.; Berthier, D.; Artzner, F.; Desbat, B.; Oda, R. *J. Am. Chem. Soc.* **2007**, *129*, 3754–3762.
(43) Snyder, R. G. *J. Mol. Spectrosc.* **1961**, *7*, 116–144.

Table 1. Peak Indexes of the Diffraction of 16-2-16 DL-Tartrate (Figure 2) in an Orthorhombic Cell[a]

h,k,l[b]	q_{cal} (I_{cal})[c]	q_{obs} (I_{obs})[c]
2,0,0	0.193 (100)	0.193 (100)
4,0,0	0.386 (4)	0.385 (7)
6,0,0	0.579 (10)	0.577 (10.5)
2,0,1	0.667 (4)	0.667 (5)
4,0,1	0.746 (4.5)	0.746 (3)
8,0,0	0.771 (16)	0.770 (20)
1,1,0	0.815 (1)	0.815 (1)
2,1,0	0.832 (2)	0.834 (1)
3,1,0	0.859 (4)	0.860 (1)
6,0,1	0.862 (4)	0.861 (1)
4,1,0	0.896	vw[d]
7,0,1	0.929	vw[d]
5,1,0	0.942 (2)	0.940 (2)
10,0,0	0.964 (6)	0.963 (6)
6,1,0	0.995	0.997 (w)[d]
8,0,1	1.001	1.007 (w)[d]
0,1,1	1.031	1.021
1,1,1	1.035	vw[d]
7,1,0	1.054	vw[d]
11,0,0	1.061	vw[d]
9,0,1	1.077	1.083 (w)[d]
8,1,0	1.118	1.119 (w)[d]
12,0,0	1.157	1.154 (w)[d]

[a] $a = 65.16$ Å, $b = 7.77$ Å, and $c = 9.84$ Å. [b] *h*, *k*, and *l* are Miller indexes. [c] q_{cal} (I_{cal}) and q_{obs} (I_{obs}) are the calculated and observed peak positions (peak intensities). Both peak intensities are normalized to the most intense peak (2,0,0). [d] w and vw mean weak and very weak intensities, respectively.

is slightly larger than the gemini molecular length (25 Å) and suggests an interdigitation of the aliphatic chains. Two non-interdigitated leaflets in the bilayer are unlikely, as they could only be accommodated at an improbable tilt angle of the alkyl chains of over 50°. The surface per aliphatic chain, $bc/4 = 19.1$ Å^2, indicates a close-packed crystalline state.[44] Among the seven known types of chain-packing in crystals of lipid bilayers, only the O′|| is a compatible sublattice of (*b*,*c*). This packing has been previously observed in crystals of oleic acid with $b_{sub} = 7.93$ Å and $c_{sub} = 4.74$ Å.[45] Thus, the aliphatic chains are parallel to *a* with a local packing similar to the triclinic $T_{||}$,[44,46] which defines two short chain−chain distances. The distance between two chains of a given gemini headgroup is shorter than 4 Å. Consequently, the headgroup can only link two aliphatic chains along the shorter interchain distance of $T_{||}$, i.e., $b/2 = 3.88(5)$ Å, and not $c/2 = 4.92$ Å.

Within a unit cell, two molecules of a single interdigitated bilayer are linked by a symmetry element with a translation perpendicular to the gemini headgroup direction, i.e., *c*. The glide mirror, *n*, is the unique symmetry element that can link the two molecules and thus crosses the aliphatic domain in its middle. The localization of the first two symmetry elements, namely the glide mirror planes *n* and *a*, imposes the localization of the two-fold screw axis 2_1 along *c* between the two bilayers in the aqueous domain. In summary, these first considerations lead to a preliminary structure where two interdigitated bilayers separated by a water gap cross the unit cell along (*b*,*c*), the alkyl chains being parallel to *a* (Figure 3a) and the headgroups being oriented along *b*.

(44) Small, D. M. *Handbook of lipid research, The Physical Chemistry of Lipids*; Plenum Press, New York, 1986.
(45) Abrahamson, S.; Ryderstedt-Nahringbauer, I. *Acta Crystallogr.* **1962**, *15*, 1261–1268.
(46) Kitaigorodskii, A. I. *Organic Chemical Crystallography*; Springer, New York, 1984.

As we have previously shown,[41] the gemini dications are intrinsically achiral but may adopt two mirror-imaged conformations at their headgroups. Both conformations are found in the ribbons. According to the planar chiral shape of the ethylene spacer from a top view, these conformations will be noted Z

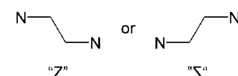

and backward-Z (in red and pink, respectively, Figure 3a). The assignment of the space group and the localization of the screw axis are sufficient to identify the chirality relationship between enantiomers in the ribbons. Each bilayer is racemic and formed by an L-tartrate leaflet and a D-tartrate leaflet that are related by the (*b*/2, *c*/2) glide mirror in the middle of the aliphatic chains. The headgroups of two consecutive bilayers that are in contact through the water gap have the same chiral conformation and are related by the screw axis. The unit cell is thus constituted by two successive racemic, heterochiral bilayers that are alternatively separated by homochiral headgroup regions where all tartrates are either L or D.

Refinement of a Model of the Racemic 16-2-16 Tartrate. As mentioned above, symmetry requirements and the size of the unit cell allowed us to locate, with some accuracy, the four molecules of 16-2-16 tartrate. To refine this structure, we then simulated the X-ray powder diffraction pattern of the resulting molecular arrangement and compared it with the experimental pattern. Several essential parameters were considered in performing the comparison. The construction of a unit cell is shown in the Supporting Information (Figure S1).

The first element is the depth of the interdigitation. The symmetry elements and the *trans* conformation of the alkyl chains require the depth of interdigitation of chains in a bilayer to be an even number of carbons. Taking into account steric considerations, the hydrophobicity of the chains, and the dimension of the unit cell ($a \approx 65$ Å), we estimated the depth of interdigitation to be 14 out of 16 carbons. Further interdigitation would result in direct contact of the chain terminal methyl group with water molecules, and lower interdigitation would not be compatible with the cell dimensions. The space that remains between consecutive bilayers is to be filled by tartrate ions and water molecules.

The relative positions of the tartrates and the gemini moieties with respect to the fully generated bilayer were then determined: the generation of multiple simulated powder spectra let us conclude that a tartrate from one leaflet is located on top of the methyl groups of the alkyl chains of the gemini from the other leaflet of the same bilayer. The relative positions and orientations of tartrate and gemini moieties in the same monolayer were then determined. We found that, when the orientation of the two ionized functions of gemini (ammoniums) and tartrate (carboxylates) is parallel, the generated powder spectrum leads to two very intense peaks at $2\theta = 14.58°$ (0,1,1) and 18.02° (0,0,2) in the simulation that are not observed experimentally. We then rotated tartrate ions relative to the gemini moiety in 5° steps, and a powder spectrum was generated at each point. The above-mentioned two peaks disappeared when the relative angle was between 90° and 95°.

Such operations allowed bilayer constructions. However, the distances between the consecutive bilayers as generated above were too large to allow any interaction between them, which resulted in a void space. Moreover, the generated powder patterns at this stage were still far from those obtained

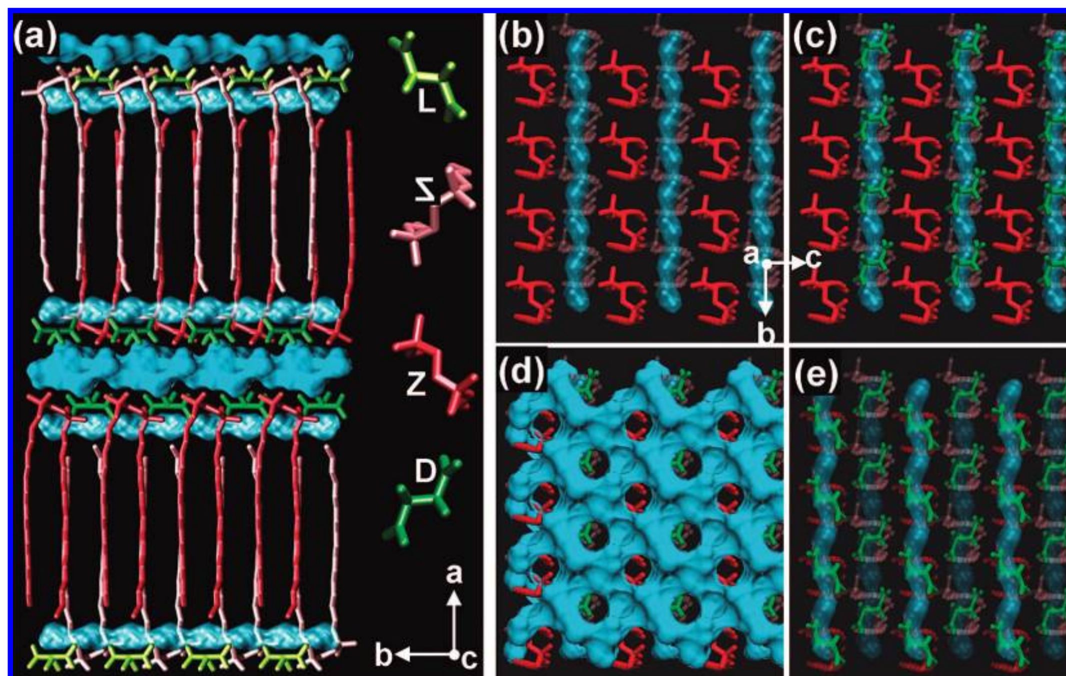

Figure 3. Molecular packing of racemic 16-2-16 tartrate giving the best fit between experimental and simulated powder diffraction patterns. (a) View from the side, along the *c* axis, and color code used to represent D- and L-tartrate as well as the two enantiomeric conformers of the gemini headgroup. (b−e) Views from the top (down the *a* axis) of the surface of a bilayer. In (b), only the gemini headgroups and water columns between them are shown. In (c) and (d), tartrate counterions and interstitial water have been successively added on top of the view in (b). In (e), the tartrate ions belonging to the opposite bilayer have been added, but interstitial water was removed for clarity.

experimentally. It was clear that solvation was required to ensure the cohesion of the structure. Fiber density helped assess their water content. Fibers dispersed in D_2O (density 1.1) sink, whereas they float in H_2O and remain suspended in D_2O/H_2O mixtures. Thus, fiber density was estimated to $\sim$1.05 $\pm$ 0.04, compatible with 4−6 water molecules in the asymmetric unit. Water molecules were introduced one by one in the model at the interface of two bilayers, and at each step a powder spectrum was generated. We observed that the number of water molecules has a particularly large influence on the intensities of peaks at $2\theta = 2.7°$ (2,0,0), 5.40° (4,0,0), 8.10° (6,0,0), 9.38° (2,0,1), and 10.82° (8,0,0). It clearly appeared that the best fit in terms of relative intensities of these peaks was found with six water molecules.

In order to accurately locate all the molecules within the crystal cell, a double bilayer built from 3×3 cell contents (i.e., 36 gemini tartrates) with six water molecules per asymmetric unit randomly located at the bilayer interface was submitted to a long minimization procedure followed by several cold (100 K) molecular dynamics runs. In order to crystallize the surrounding space, a full image convention was used for the periodic boundary conditions. It was observed that the two alkyl chains of each gemini slightly deviate from the initial parallel orientation. The tartrate position and orientation remained essentially unchanged.

This minimized gemini amphiphile conformation was then used again to finely locate water molecules. We found that the positions of the water molecules are crucial for the quality of the fit between the generated pattern and the experimental data. Meanwhile, to position correctly the water molecules in three-dimensional space turned out to be the most challenging task. At the beginning, the six water molecules were positioned randomly at the interface between the two bilayers. A double bilayer built from 3×3 cell contents was again generated and fully minimized using a conjugate gradient and a full image convention for periodic boundary conditions. During the minimization, the positions of gemini and tartrates were fixed in the first 2000 steps and tethered with a constraint of 200 kcal/Å^2 in the next 1000 steps. We then performed several short and cold (100 K) molecular dynamics runs. During these runs, we found that two of the six water molecules migrated below the top of the gemini headgroups to settle between the tartrates and the terminal methyl groups of the alkyl chains. At the end of the dynamic simulation, these water molecules form an undulating linear arrangement (Figure 3b, in transparent blue). The remaining four water molecules (shown in opaque blue) organize into two parallel planes in the gap between the bilayers, separated from the tartrate layer by roughly 2 Å (Supporting Information, Figure S2). In the $Pna2_1$ symmetry, these four water molecules form a two-level hexagonal lattice. Such an organization strongly suggests the presence of a network of hydrogen bonds between the tartrate ions of one leaflet and the tartrate ions of the opposite leaflet. The plane defined by each carboxylate moiety of the tartrate ions is oriented almost perpendicular to the membrane surface. One oxygen atom points toward the bilayer, where a second set of water molecules (two per gemini) is organized in undulating lines (Supporting Information, Figure S3). These columns of water molecules apparently form hydrogen-bonded bridges between two carboxylate oxygens belonging to the same tartrate molecule, or to neighboring tartrate molecules. The other oxygen atom from the carboxylate moiety, along with the hydroxy groups, points away from the bilayer to the hexagonally packed water layer. At this stage the calculated powder spectrum is very close to the experimental spectrum up to $2\theta = 15°$, except for a small discrepancy for the peak at 5.40°, which can be due to some disorder-induced peak broadening (52% of the measured value, whereas the other peaks are within 15% of the measured value,

as seen in Table 1). As we have mentioned above, to find the positions of six water molecules per gemini–tartrate while respecting the symmetry group turned out to be extremely difficult but crucial for a good fit between the experimental diffraction pattern and the simulated pattern, revealing the importance of the solvent molecules in the crystalline structure. Despite the fact that the X-ray data do not have the necessary resolution to unambiguously confirm the position of water molecules, we believe that the results from molecular modeling studies, in particular the spontaneous segregation of water molecules into two ensembles both consistent with crystallographic symmetry operations, can hardly be artifacts.

Additional Features of the Racemic 16-2-16 Tartrate Structure. Aside from the features described in the two sections above—interdigitation, the heterochiral nature of each bilayer, the absence of alkyl chain tilt, and the positions of tartrates and water molecules—several aspects of the racemic structure deserves comment.

Each tartrate dianion adopts an anti conformation and lies flat in a cavity at the bilayer surface between adjacent gemini headgroups and above the end of the alkyl chains belonging to the other leaflet. They are at the same height as the ammonium headgroups (Figure 3a). The gemini headgroups being homochiral within one leaflet, the cavities between them are chiral as well and may host only one enantiomer of the tartrate. All tartrate molecules in the same monolayer are oriented parallel to each other (Figure 3c). Water molecules are present in two distinct zones and seem to play a crucial role in bridging tartrates through hydrogen bonds.

The high cohesion between the individual chiral units of the ribbon structure is likely at the origin of the expression of chirality at the scale of the entire ribbon (Figure 1). Specifically, two elements of cohesion, one heterochiral and one homochiral, allow us to speculate about the mechanisms of chirality transfer. First, the interdigitation of hydrophobic tails of gemini is key for transferring chirality from one leaflet (monolayer) to the other within a bilayer. The steric constraint of tightly packed interdigitated bilayers requires that the two leaflets are heterochiral. Second, gemini headgroups, tartrates of a single configuration, and water molecules are tightly interconnected through hydrogen and ionic bonds and as well as steric interactions and ensure the cohesion between two bilayers.

The 16-2-16 Tartrate Single-Enantiomer Structure. Homogeneous gels of the pure L enantiomer in water (10% w/w) were investigated by high-resolution X-ray scattering (Figure 4) both as twisted ribbons (fresh gels) and as helical ribbons (aged gels). Diffraction patterns are identical for helical and twisted ribbons.

They exhibit broad diffuse scattering in SAXS as well as in WAXS that indicates the absence of three-dimensional crystalline order. The minima of the SAXS modulations are in good agreements with a cosine function and have been already observed in the case of double-walled nanostructures.[47] Observed repeat distances of around 32 Å as well as TEM observations (Figure 1c) strongly suggest that the ribbons are made of exactly two similar bilayers, as found in the unit cell of the racemic structure. Moreover, the maxima of WAXS diffuse scattering are close to those of the racemic main Bragg peaks, suggesting a similar molecular packing. This hypothesis was validated upon fitting the full data set with an electron density model for the SAXS and free position and intensities peaks for WAXS (Figure 4). The diffuse scattering intensity was fitted by the sum of two independent functions corresponding to the small-angle X-ray scattering, I_{SAXS}, and the wide-angle X-ray scattering, I_{WAXS}:

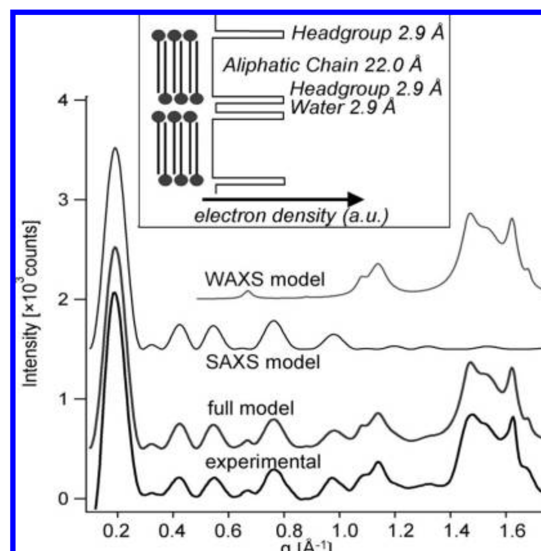

Figure 4. X-ray diffuse scattering pattern of an aqueous suspension of flat ribbons of enantiomer 16-2-16 tartrate, 10% w/w at 20 °C (bottom). The model is the sum of a SAXS model and a WAXS model. The SAXS model results from the electron density perpendicular to the membrane and indicates the double-bilayer structure of the ribbons. The WAXS model results from the in-plane packing of the geminis.

$$I_{SAXS}(q) = I_{norm}[\cos(qe/2)]^2\left[\frac{\sin[q(d_c/2 + d_{hg})]}{q(d_c/2 + d_{hg})} + (\rho - 1)\frac{\sin(qd_c/2)}{qd_c/2}\right]^2 / q^2$$

where $e = 32.48$ Å is the membrane thickness, which corresponds to the repeat distance between the two membranes, $d_c = 22.05$ Å is the thickness of the aliphatic chains, $d_{hg} = 2.9$ Å is the thickness of the headgroup, and $\rho = -0.05$ is the relative electron density, with electron density of water equal to 0 and electron density of the headgroup equal to 1.

$$I_{WAXS}(q) = \sum_i \frac{I_i}{1 + [(q - q_i)/\Delta q_i]^2}$$

where I_i is the intensity, q_i the position, and Δq_i the half-width at half-maximum of the ith WAXS peak. The values are given in Table 2. The $(h,k,l)_{DL}$ Miller indexes of the DL crystal are given for comparison.

The electron density profile shown Figure 4 (inset) confirms the presence of two identical bilayers, each with a thickness of 32.5 Å. The distance between consecutive high electron density areas corresponding to the tartrate headgroup is 24.9 Å. These distances match those observed for the racemic multilayer ribbons within 0.3 Å. The WAXS diffuse scattering positions show very good agreement with the racemate peak positions (Table 2), and the systematic extinction confirms that molecular packing is identical in the ribbons of the pure enantiomers and

(47) Pouget, E.; Dujardin, E.; Cavalier, A.; Moreac, A.; Valérie, C.; Marchi-Artzner, V.; Weiss, T.; Renault, A.; Paternostre, M.; Artzner, F. *Nat. Mater.* **2007**, *6*, 434–439.

Table 2. Peak Indexes of 16-2-16 L-Tartrate Powder Diffraction Pattern with the Same Unit Cell as the DL Crystal

$(h,k,l)_{DL}^{a}$	q_{obs}^{b}	I_{obs}^{b}	Δq_{obs}^{b}
(2,0,1)	0.669	14	0.017
(6,0,1)	0.88	2	0.010
(2,1,1)	1.08	21	0.020
(4,1,1)	1.14	57	0.038
(8,0,2)	1.47	100	0.036
(2,1,2)	1.54	96	0.067
(0,2,0)	1.62	99	0.022
(4,2,0)	1.68	20	0.011
(8,2,0)	1.79	3	0.015

[a] Miller indexes. [b] q_{obs}, I_{obs}, and Δq_{obs} are observed peak positions, peak intensities, and peak widths, respectively.

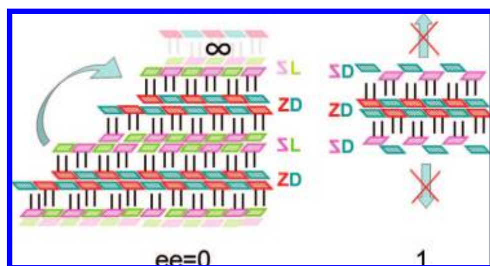

Figure 5. In the racemate (ee = 0) structure, the contact layer between two consecutive gemini bilayers is always homochiral (same gemini conformation, same tartrate configuration). This packing is possible with a pure enantiomer only for the internal adjacent leaflets. However, in the external leaflets of this double-bilayer ribbon, the conformation of the gemini headgroups is opposite to that found between the bilayers, preventing further stacking.

the ribbons of the racemate. The limited size of the crystals is at the origin of the peak broadening, as observed in nanocrystals.[48]

Symmetry at the Molecular Level and Aggregate Morphology. Our analysis leads to the conclusion that the unit cell and the symmetry elements of molecular packing and thus structural features such as two heterochiral bilayers per unit cell, comprised of homochiral monolayers, are conserved through large morphology transitions from racemic, flat multilayered ribbons to chirally twisted, helical ribbons as well as tubules of the pure enantiomer. These insights into the molecular-scale packing within membrane ribbons shed light on a number of macroscopic features.

Indeed, the structure of the pure enantiomer ribbons which are composed of exactly two bilayers (Figure 1c) can be understood on the basis of the packing mode of chiral elements discussed above in the case of the racemate structure. We have seen that the contact domain between adjacent bilayers is homochiral: both gemini headgroups and tartrate of the symmetrical leaflet have the same chirality (Figure 5). In the racemate, the infinite alternation of domains between bilayers having D(backward-Z)D(backward-Z) and LZLZ arrays of headgroups and tartrate ions is possible without chirality frustration. In contrast, in the case of a pure enantiomer (L for instance), only two bilayers can stack, separated by a domain with an LZLZ array of headgroups and tartrate ions. In the external leaflets of these double-bilayer ribbons, the heterochiral bilayer packing requires that the gemini conformation is backward-Z, and obviously, the only available tartrate (L) cannot be accommodated within the chiral cavity where D tartrates are expected.

(48) Guinier, A. *X-ray Diffraction in Crystals, Imperfect Crystals, and Amorphous Bodies*; Dover Publication: New York, 1994; pp 219–237.

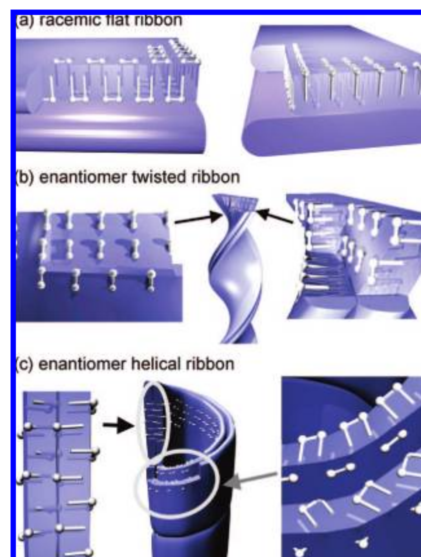

Figure 6. Schematic representation of the orientation of gemini molecules with respect to the ribbons in (a) flat, (b) twisted, and (c) helical structures.

Now let us compare the symmetry of the molecular packing as obtained from X-ray analysis and the symmetry of the final aggregates such as tubular, helical, or twisted ribbons. We know first that the axis *a* of the unit cell should be perpendicular to the bilayer plane. Additionally, the peak indexed as (0,2,0) in the diffraction pattern shown in Figure 4 is particularly sharp, indicating a long-range order (∼80 nm) along the *b* axis direction. This is longer than the ribbons' width, suggesting that the *b* axis is oriented parallel to the long axis of the ribbons, and consequently the *c* axis is oriented along the width of the ribbons. A result of this is that the gemini headgroups are also oriented parallel to the long edge of the ribbons,[49] as we had speculated in previous studies.[50,51]

Orienting the unit cell, i.e., molecular packing, with respect to the ribbon allows us to establish possible correlations between symmetry elements at molecular and mesoscopic scales. In particular, the crystallographic C_2 axis along *c* crosses the ribbons along their width. We note that this local molecular symmetry also exists at the scale of the whole aggregate in the cases of flat (Figure 6a) and twisted ribbons (Figure 6b), but not in the helical ribbons (Figure 6c) because in the latter, the long axis of the ribbons (*b*) does not coincide with the macroscopic long axis of the helix itself. This suggests that the transition in morphology from twisted to helical ribbons/tubules amounts to a symmetry-breaking.

Mechanism of the Expression of Supramolecular Chirality. The molecular organization of the ribbons of 16-2-16 tartrate also refers to how and why they adopt a twisted or helical shape when they are enantiomerically enriched. As shown in Figure 3, tartrate molecules and Z or backward-Z chiral headgroups

(49) As shown in Figure 3b, the N−N axis of each headgroup is not exactly parallel to *b* but the plane defined by the two chains of each gemini is parallel to *b* and thus to the long edge of the ribbon.

(50) Oda, R.; Laguerre, M.; Huc, I.; Desbat, B. *Langmuir* **2002**, *18*, 9659–9667.

(51) Oda, R.; Huc, I.; Homo, J.-C.; Heinrich, B.; Schmutz, M.; Candau, S. *Langmuir* **1999**, *15*, 2384–2390.

of the gemini define arrays of preferred orientations that deviate from the ribbon long and short axes. For example, the carboxylate-carboxylate direction of each tartrate is almost parallel to (0,1,1) that is at an angle of $\sim$38° from the ribbon long axis. Such arrays are susceptible to generate tensions, attractive or repulsive, at the ribbon surface. Importantly, the orientation of these arrays is not the same on either side of the water gap between two bilayers. If one array is oriented at $\sim$38° with respect to *b*, the other is oriented at $\sim -38°$. Therefore, tensions are exerted in a crossed manner on the two sides of a double bilayer ribbon. Such tensions are expected to be released upon a chiral deformation of the ribbon. If the tensions on the two sides remain equal in the process, a twisted shape with saddle-like curvature will result, whereas if the tension becomes larger on one side than on the other, a helical shape with cylindrical curvature will result.

In turn, bending or twisting results in frustrations of molecular packing. As can be seen in Figure 6b,c, the curvatures inherent to twisted or helical ribbons are conducive to surface area variations which can be accommodated by variable molecular tilts. Introducing a twist into a flat ribbon implies that the area per molecule should be larger close to the long edges of the ribbons than in the middle. One simple way to increase surface area while preserving molecular organization and crystalline chain-packing is to introduce a molecular tilt perpendicular to *c*, in the (*a*,*b*) plane (Figure 6b). Conversely, in the case of helical ribbons, the area per molecule should be larger in the external bilayer than in the internal bilayer. Again, this frustration can be resolved by introducing a molecular tilt in the external bilayer. Tilt angles, of course, have an upper limit beyond which bilayer integrity does not hold. Indeed, this may well be the main factor that limits the width of twisted ribbons.

Conclusion

The pseudo-crystalline character of the racemic mixture of 16-2-16 tartrate multi-bilayer self-assembled ribbons makes them suitable for X-ray powder diffraction investigations, which together with molecular dynamics simulations have allowed us to elucidate their structure. A detailed molecular organization is proposed where gemini molecules and tartrate ions as well as water molecules are all accurately positioned in the hydrated state. Essential features of this organization include interdigitation of alkyl chains within each bilayer and networks of ionic and hydrogen bonds between cations, anions, and water molecules between bilayers. This results in the molecular packing following the symmetry leading to homochiral monolayer, heterochiral bilayer, and heterochiral adjacent bilayers conserved through large morphology transitions from racemic flat multilayered ribbons to chirally twisted and helical ribbons as well as tubules of the pure enantiomer.

The structure thus possesses a high cohesion, which is likely at the origin of the expression of molecular chirality at a mesoscopic scale in this system. The organization of the ribbons at the molecular level allows to understand a number of their macroscopic features. Among these are the reason why enantiomerically pure 16-2-16 tartrate forms ribbons that consist of exactly two bilayers and a plausible mechanism by which a chirally twisted or helical shape may emerge from the packing of chiral tartrate ions. Importantly, the distinction between commonly observed helical and twisted morphologies appears to emerge from a simple symmetry-breaking.

Our results demonstrate that solving the molecular structure of relatively soft self-assembled materials is now within reach and that it is a valid approach to correlate molecular parameters to macrocopic properties.

Experimental Section

X-ray Scattering. Samples at 10% in Millipore water (w/w) were put in glass capillaries (Glas, Muller, Berlin). Experiments were performed at station D43 at the LURE synchrotron (France) using a monochromatic (1.451 Å) focused X-ray beam selected by a parabolic Ge(111) crystal. The beam was defined by a 120 cm collimator. The X-ray diffraction patterns were recorded, at exposure times of 30−50 min, using a decentered image plate (15 × 20 cm^2) which was further digitized for analysis. The sample-to-detector distance of 245 mm was used to give high-resolution patterns. All samples exhibited powder diffraction Debye−Sherrer rings. Hence, the scattering intensities as a function of the radial wave vector, $q = 4\pi \sin(\theta)/\lambda$, were determined by circular integration.

Molecular Modeling. Calculations were performed on an SGI Octane workstation running Insight II and Discover version 2000 (Accelrys Inc.) software, and molecular dynamics runs were performed on a quadriprocessor SGI Origin 200 server. All analyses were performed within the Decipher and Analysis modules of the Insight package. For van der Waals and electrostatic treatment, we used a group-based cutoff of 35 Å.

All powder spectra calculations and the whole crystallography study were performed with Mercury v. 1.3 from the CCDC (Cambridge), using the symmetry elements of the cell group $Pna2_1$ (No. 33).

Acknowledgment. This work was supported by the Conseil Régional d'Aquitaine, Centre National de la Recherche Scientifique, and the French Ministry of Research. We thank Dr. Dominique Durand for the high quality of her technical support during experiments performed on D43 at the LURE synchrotron.

Supporting Information Available: Additional experimental information as described in the text. This material is available free of charge via the Internet at http://pubs.acs.org.

JA8048964